Collagen Microstructural Factors Influencing Optic Nerve Head Biomechanics

Liang Zhang,[1,2] Julie Albon,[3] Hannah Jones,[3] Cecile L. M. Gouget,[4] C. Ross Ethier,[5] James C. H. Goh,[6] and Michaël J. A. Girard[2,7]

[1]NUS Graduate School for Integrative Sciences and Engineering, National University of Singapore, Singapore
[2]In vivo Biomechanics Laboratory, Department of Biomedical Engineering, National University of Singapore, Singapore
[3]Optic Nerve Head Group, School of Optometry and Vision Sciences, Cardiff Centre for Vision Sciences, Cardiff University, Cardiff, United Kingdom
[4]LadHyX, Department of Mechanics, École Polytechnique, CNRS UMR7646, Palaiseau, France
[5]Wallace H. Coulter Department of Biomedical Engineering, Georgia Institute of Technology and Emory University, Atlanta, Georgia, United States
[6]Tissue Repair Laboratory, Department of Biomedical Engineering, National University of Singapore, Singapore
[7]Singapore Eye Research Institute, Singapore National Eye Centre, Singapore

Correspondence: Michaël J.A. Girard, In vivo Biomechanics Laboratory, Department of Biomedical Engineering, National University of Singapore, 9 Engineering Drive 1, Block EA #03-12, Singapore 117576; mgirard@nus.edu.sg.

Submitted: September 24, 2014
Accepted: February 23, 2015

Citation: Zhang L, Albon J, Jones H, et al. Collagen microstructural factors influencing optic nerve head biomechanics. *Invest Ophthalmol Vis Sci*. 2015;56:2031–2042. DOI:10.1167/iovs.14-15734

Purpose. Previous studies have suggested that the lamina cribrosa (LC) and its surrounding sclera are biomechanically important in the pathogenesis of glaucoma, but many were limited by assumptions of tissue isotropy and homogeneity. Here, we used an improved biomechanical model driven by experimental measurements of scleral and LC collagen fiber organization to more accurately evaluate optic nerve head (ONH) biomechanics.

Methods. Collagen fiber organization was quantitatively mapped across human ONH cryosections (three normal and three glaucomatous) using small-angle light scattering (SALS) and fed into two-dimensional finite element models loaded under biaxial stress to simulate raised intraocular pressure. Effects of artificial variations in collagen fiber microstructure and stiffness on LC and scleral strains were also investigated.

Results. Scleral collagen fibers were circumferential and exhibited the highest alignment in a region not immediately adjacent to, but at a distance (400–500 μm) away from, the LC. In models, such a fiber arrangement yielded rings of low strain (second principal and effective) in the scleral region immediately adjacent to the LC. Further sensitivity analyses showed that scleral fiber alignment was crucial in determining LC strain levels. Moderate scleral anisotropy (as observed physiologically) was more effective than isotropy or high anisotropy in limiting LC and scleral strain magnitude.

Conclusions. The presence of a heterogeneous collagen fiber organization in the peripapillary sclera appears effective in limiting LC strain and is able to reduce strain levels at the scleral canal boundary: a transition zone prone to LC disinsertion, focal lamina cribrosa defects, and optic disc hemorrhages in glaucoma.

Keywords: optic nerve head biomechanics, finite element modeling, collagen microstructure, glaucoma, ocular biomechanics

Glaucoma is the second leading cause of blindness worldwide, following cataract.[1] It is primarily a disease of the elderly, characterized by irreversible damage to the retinal ganglion cell axons within the ONH,[2] where the axons pass through the LC and exit the eye. While glaucoma has been historically associated with elevated intraocular pressure (IOP),[3–5] varied sensitivity to IOP has been observed.[6,7] We have thus hypothesized that it is the biomechanical environment that plays an important role in glaucoma, whereby biomechanically "weak" eyes may exhibit large IOP-induced ONH deformation that could eventually lead to ganglion cell axonal loss.[7–9] The sclera is the stiffest ocular tissue and its main load-bearing structure. Studies have shown that the sclera and the LC are biomechanically coupled,[10–12] and the stiffness of the sclera strongly influences the IOP-induced deformation experienced by the LC.[13,14]

Direct biomechanical measurements of the ONH in vivo are not yet feasible, although several techniques are underway.[15,16] Computational modeling (e.g., finite element or FE) is an alternative approach to predict the biomechanical environment of the ONH. Initial FE models of the ONH were mostly generic, and parametric studies have been performed to investigate the main determinants of ONH biomechanics.[7,11,12,14] Individual-specific models were also developed based on morphologic reconstructions of human and monkey ONHs.[13,17] However, most studies have assumed homogeneous and isotropic linear elastic mechanical properties of the eye tissues, which is an unrealistic simplification. The sclera and LC are nonlinear, anisotropic (stiffness varies with orientation), and heterogeneous (stiffness varies spatially) tissues.

The primary structures that provide the sclera with mechanical strength are lamellae of type I collagen fibers,[18]

Table. Demographics of Donor Eyes

Donor	Age, y	Sex	Mean Deviation, dB	Cup/Disc Ratio
N1 R	88	F	—	—
N2 L	88	F	—	—
N3 L	87	M	—	—
G1 R	86	M	−1.54 in 2002	Unknown
G2 L	87	F	−12.81 in 2008	0.9
G3 L	73	M	Unknown, diagnosed in 2007	Unknown

Eyes from donors diagnosed with primary open angle glaucoma ($n = 3$ eyes total, G1–G3, donor ages ranging 73–87 years) received from the Mayo Clinic and age-matched control eyes ($n = 3$ eyes total, N1–N3, with no known ocular pathology, aged 88, 88, and 87 years, respectively) received from Bristol Eye Bank (Bristol, UK). Note that glaucoma eyes used in this study were donated by subjects diagnosed with glaucoma by a trained glaucoma specialist. All patients were taking IOP-lowering medications at the time of death. R, right eye; L, left eye.

which are buckled initially and uncrimp with stretch,[18] leading to increased stiffness at high IOP levels. This nonlinear mechanical behavior has been observed experimentally in the sclera.[10,18–21] The anisotropy of the sclera is mainly due to the alignment of collagen fibers. Specifically, it has been reported that in rat,[22] monkey,[23] and human[24,25] eyes, the sclera is anisotropic with circumferential collagen fiber alignment near the ONH and is isotropic at the equator. This also suggests that the sclera is heterogeneous. Thus, to better understand ONH biomechanics, it is crucial to incorporate information about collagen fiber organization into computational modeling. This was achieved by recent computational studies that took into account collagen microstructure[10,26,27] and remodeling.[28,29] Others have used inverse FE to predict collagen fiber organizations from experimental inflation data.[23,30–32] However, none of these studies have been able to incorporate experimental measurements of collagen fiber organization for both the sclera and the LC simultaneously.

In this study, we incorporated fiber organization information (sclera and LC) from postmortem human eyes, measured by SALS, within nonlinear heterogeneous anisotropic FE models of the ONH. Our aim is to investigate the mechanical role of collagen fibers in protecting the ONH from excessive deformation.

Materials and Methods

Sample Preparation

Three control human eyes (from Corneal Transplant Service Bristol Eye Bank, Bristol, UK; labeled as N1, N2, and N3, without ocular pathology [Table]) and three glaucoma eyes (from Mayo Clinic, Rochester, NY, USA; labeled as G1, G2, and G3 [Table]) were dissected, and their ONHs serially cryosectioned transversely. All tissues were immersion fixed in 4% paraformaldehyde within 48 hours postmortem. Experimental procedures complied with the UK Human Tissue Act regulations and were approved by the South East Wales Research Ethics Committee. All slices were additionally subjected to second harmonic generation (SHG) imaging, and only one 100-μm cryosection was selected from the "central" region of each ONH while ensuring it incorporated the peripapillary sclera and the "central" LC but not the pre- and postlaminar tissues. Note that we used transverse cross-sections to capture the majority of scleral and LC collagen fibers, as such fibers primarily (but not exclusively) run tangentially to their respective tissue surface.[33,34]

Small-Angle Light Scattering (SALS)

The fiber organization of the LC and peripapillary sclera was characterized by SALS using an experimental setup (Fig. 1a) we have previously validated.[22,35–37] Briefly, each ONH cryosection was raster scanned (spatial resolution or distance between two scanning points: 100 μm) with a 5-mW nonpolarized HeNe

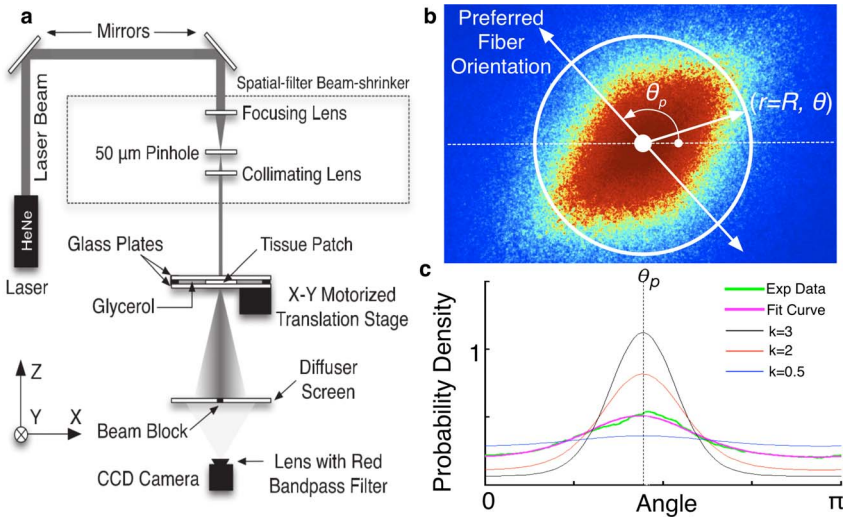

Figure 1. (a) Experiment setup of SALS. (b) Typical SALS pattern. The normalized light intensity, which is a function of angle θ at a fixed radius $r = R$, is proportional to the fiber angular probability distribution, shifted by 90°. (c) Angular fiber distribution. The angle at which the peak value occurs is the preferred fiber orientation θ_P. The fiber distribution is π periodic. Experimental data (*green curve*) are fitted by a constrained von Mises distribution function (*purple curve*). Functions with different k values are also plotted (see text). A larger k value indicates more aligned fibers along θ_P. Figure adapted with permission from Girard MJA, Dahlmann-Noor A, Rayapureddi S, et al. Quantitative mapping of scleral fiber orientation in normal rat eyes. *Invest Ophthalmol Vis Sci*. 2011;52:9684–9693.[22]

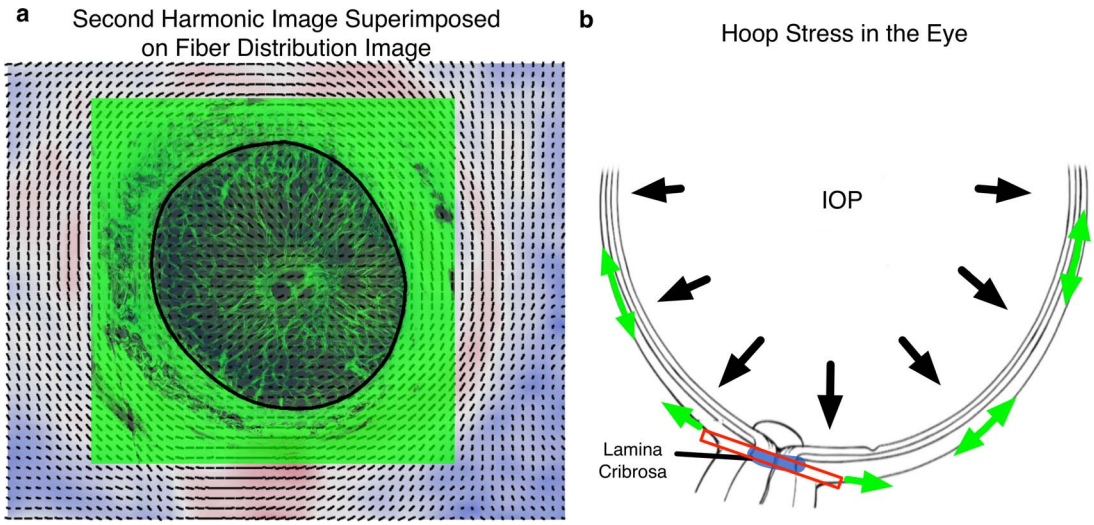

FIGURE 2. (**a**) Second harmonic image superimposed on the SALS fiber map to aid segmentation of the LC (*black delineation*). In this SALS fiber map, each *black segment* represents the preferred fiber orientation, and the length is modified to be proportional to its corresponding fiber concentration factor. (**b**) The primary load experienced by the ONH is the in-plane hoop stress (*green arrows*), resulting from the IOP (*black arrows*). For each chosen section of the ONH (region within *red rectangle*, enclosing the LC, shown in *blue*), 2D biaxial stress models were created to mimic the IOP-induced hoop stress.

laser (model 1125; JDS Uniphase Corp., Milpitas, CA, USA). A customized spatial-filter beam-shrinker assembly (modified from KT310/M; Thorlabs, Inc., Newton, NJ, USA) was used to generate a laser beam diameter of ~300 μm. Scattered light (primarily from collagen/light interactions) was projected onto a diffuser screen behind the specimen. A blackout beam block at the center of the diffuser screen blocked the intense, nonscattered light. The scattering pattern was captured by a charge-coupled device (CCD) camera (resolution: 1024 × 768 pixels, 8–16 bits; model B953; PixeLINK, Ottawa, ON, Canada) positioned behind the diffuser screen. A low-distortion/high-resolution lens (NT56-788; Edmund Optics, Barrington, NJ, USA) and a red band-pass filter (model FL632.8-3; Thorlabs, Inc.) were mounted on the camera to reduce noise. For a given cryosection of 4.5 × 5 mm, 2346 images were acquired.

For thin soft tissue applications, SALS is able to detect the orientation of collagen fibers and collagen fiber bundles.[35,37] Since our laser beam spot is 300 μm in diameter, all the collagen fibers and collagen fiber bundles within that area (peripapillary sclera or LC) will contribute to the fiber distribution at any given scanning point.

Quantitative Mapping of Collagen Fiber Distribution

From each scattering pattern image (Fig. 1b), light intensity was derived and normalized to describe the angular distribution of collagen fibers within the plane of the section (Fig. 1c, green curve).[38] In order to extract microstructural parameters for use within FE models, each experimentally derived fiber distribution was fitted with a modified π-periodic von Mises distribution P, expressed as

$$P(\theta) = \frac{1-\beta}{\pi} + \frac{\beta}{\pi I_0(k)} \exp(k\cos(2(\theta - \theta_P))), \qquad (1)$$

where θ_P is the preferred fiber orientation (describing the main orientation of the collagen fibers within the plane of the section; Fig. 1c, dotted line), β is a parameter between 0 and 1 that weights the proportion of isotropic and anisotropic contributions, k is the fiber concentration factor (characterizing the fiber spread around θ_P), and I_0 is the modified Bessel function of the first kind of order zero. To get a unique fit for the distribution function, the parameters β and k were constrained such that

$$\beta = \left(\frac{I_1(k)}{I_0(k)}\right)^n, \qquad (2)$$

where I_1 is the modified Bessel function of the first kind of order 1, n is a tissue-dependent parameter, and $n = 1$ was used here as recommended by our previous work.[38] The error between $P(\theta)$ and the experimentally derived fiber distribution was minimized using differential evolution optimization,[39] to obtain a unique pair of microstructural parameters (θ_P and k) at each scanning point (Fig. 1c, purple curve). On average, errors (area difference between the fitted and experimentally derived distributions) were 0.054 ± 0.030. Fiber organization maps were then constructed for each ONH (θ_P values represented by line segments, and k values represented by contour colors; Figs. 2a, 3).

Note that the constrained von Mises distribution (Equation 1) was chosen as it was found to better describe fiber alignment by taking into account a significant isotropic contribution[38] often observed in thin soft tissues.[40,41] It is thus more representative than the standard von Mises distribution in describing collagen microstructure in thin soft tissues.[10,23,29,42,43]

FE Simulation and Constitutive Model

To understand how collagen fiber microstructure influences IOP-induced ONH deformations, two-dimensional (2D) FE models (Supplementary Fig. S4) were created. All models incorporated the experimentally derived measurements of collagen fiber organization (θ_P and k), which were interpolated (cubic spline) and assigned to corresponding model elements. Each SHG image[22] was colocalized with its respective SALS map (using central retinal vessels and posterior ciliary arteries as landmarks) to obtain clear boundaries between the LC and the sclera (Fig. 2a). Each FE model (one for each ONH) was subjected to 2D biaxial stress loading as the largest IOP-induced load component resisted by the ONH is within the transverse plane (i.e., the plane of the section; Fig. 2b). Such

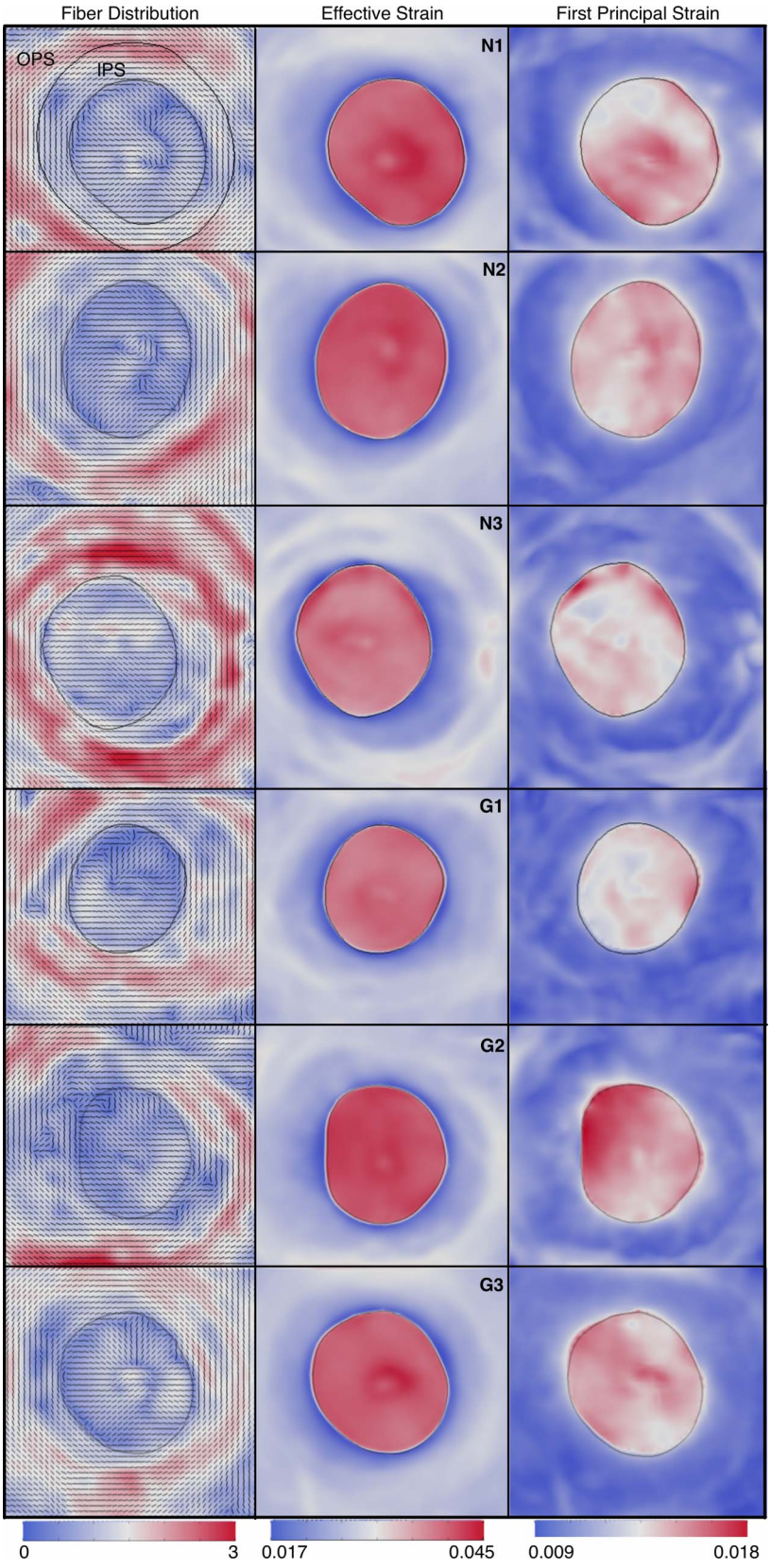

Figure 3. Preferred fiber orientation and fiber concentration factor plots (*left column*, contour color represents the magnitude of the concentration factors, while the *black line segments* represent the preferred fiber orientations); effective strain plots (*middle column*, contour color represents the magnitude of strains); and first principal strain plots (*right column*, contour color represents the magnitude of strains) for six ONH sections. The boundary of the LC is shown in *black*. The *top left plot* shows that sclera is divided into the IPS (the region outside the LC but within a radius four-thirds times that of the LC, containing the LC insertion sites into sclera) and the OPS (the region outside the IPS).

Investigative Ophthalmology & Visual Science

loads are often referred to as hoop stresses and are significantly higher than IOP itself.[44] A load of 100 kPa (as observed in monkey eyes[45] that represents ×50 IOP for a baseline IOP value of 15 mm Hg or as estimated in human eyes that represents ×27 IOP[44] for a baseline IOP value of 27.8 mm Hg) was applied to the four sides of each section to mimic the effects of IOP elevation. We note that "rectangular" loading conditions (as performed herein) are equivalent to "circular" loading conditions, as both can generate a state of a biaxial stress within the ONH. For further analyses, each ONH was divided into three subregions (Fig. 3): the LC, the inner peripapillary sclera (IPS, the scleral region immediately adjacent to the LC, defined to start at the scleral canal margin and end at a boundary with a radius equal to four-thirds times that of the LC), and the outer peripapillary sclera (OPS, the remaining sclera other than the IPS).

In order to predict ONH deformations using FE models, it is important to provide a relationship that links stress (measure of internal force) to strain (measure of deformation). To this end, an anisotropic hyperelastic constitutive equation[10] was used, as such an equation can describe the sclera and the LC as fiber-reinforced composites and be fed with experimentally determined local fiber distribution information (θ_P and k). Four extra stiffness parameters were required to fully estimate how the scleral and LC tissues would deform under mechanical stress: the first Mooney–Rivlin coefficient c_1, the exponential fiber stress coefficient c_3, the fiber uncrimping coefficient c_4, and the bulk modulus K; c_1 describes the stiffness of ground substance matrix (all tissue components and molecules except fibrous components), while c_3 and c_4 describe the stiffness of the collagen fibers.[46] K is a measure of resistance to uniform compression, and a value of 1GPa was used throughout this study to ensure tissue incompressibility.[10]

All finite element models were solved using the FEBio software package[47] (Musculoskeletal Research Laboratories, University of Utah, Salt Lake City, UT, USA) with eight-node hexahedral elements. Convergence tests were performed to assess the numerical accuracy of the FE models. Adequate accuracy (strain error within 1% of full convergence) was achieved with an averaged element length of 25 μm. Note that ONHs were in different section sizes. However, an initial assessment showed that applying surface stress to a section or a slightly cropped section had little impact on the overall predicted strain patterns.

Sensitivity Studies

To further investigate the role of collagen fiber microstructure in the mechanical response of the ONH to IOP, artificial variations in microstructural parameters, θ_P and k, were imposed, while all other stiffness parameters were fixed ($c_1 =$ 100 kPa, $c_3 = 5$ kPa, $c_4 = 400$ for the sclera, which are typical values for primate sclera[10,32]; $c_1 = 50$ kPa, $c_3 = 2.5$ kPa, $c_4 = 100$ for the LC, which are estimations based on several previous studies,[10,11,19,32] since nonlinear stiffness measurements for the LC are not available[30]). Specifically, to evaluate the effect of fiber concentration factors on ONH strain distributions, k values in the LC or in the sclera were multiplied by a scaling factor of 0, 0.5, or 2. These scaling factors were chosen to allow for artificial variations within an acceptable physiological range. To evaluate the effect of preferred fiber orientations on ONH strain distributions, θ_P values were modified to represent either circumferential or meridional organizations in the LC or in the sclera.

To investigate the role of fiber stiffness, the constitutive parameters were also varied, with k and θ_P kept as experimentally extracted. Specifically, values for c_1, c_3, and c_4 were multiplied by a scaling factor of 0.5 or 2.

Mechanical Response of the ONH to Stress

The effective strain (a scalar quantifying the tissue structural distortion[19]) distribution and the first principal strain (a scalar representing the maximum tissue stretch) distribution were examined. Strain distributions for one characteristic eye sample (G1) are presented as violin plots to illustrate the effects of artificial variations. Peak strain was defined as the 95th percentile strain in order to eliminate the influence of outliers. The 50th percentile strain values were used to indicate the median strains. Repeated measures ANOVA with Greenhouse–Geisser correction were performed to test the significance of artificial variations (null hypothesis: no difference in strain distribution due to artificial variations; details discussed in the Supplementary Material). Post hoc analyses using Scheffe's procedures were also performed when identifying pairwise difference was warranted.

Normal Versus Glaucoma ONHs

Due to our small sample size (no glaucoma: 3; glaucoma: 3), a robust statistical analysis could not be performed to evaluate the differences in scleral and LC strain distributions between normal and glaucoma eyes. Only mean values and standard deviations were reported for the LC.

Results

Collagen Fiber Organization in the LC and Peripapillary Sclera

The fiber organization maps for six ONHs are shown in Figure 3, where the color contours represent the fiber concentration factors (blue: random alignment; red: strong alignment) and the black line segments represent the preferred fiber orientations. For all ONHs, rings of circumferentially aligned fibers were observed in the peripapillary sclera around the LC, while radially aligned fibers were observed within the LC. Across all eyes, the LC exhibited lower anisotropy than that in the peripapillary sclera (average fiber concentration factor: 0.85 ± 0.26). The highest anisotropy in the peripapillary sclera was observed in the OPS region (average fiber concentration factor: 1.50 ± 0.47), which decreased in the IPS region (average fiber concentration factor: 1.27 ± 0.37).

Responses From Original ONH Configurations

Computed peak and mean strains were higher in the LC and lower in the peripapillary sclera for all ONHs (Fig. 3). A ring of low effective strain was observed within the IPS around the LC (insertion region). The mean effective strain based on the six samples was 3.87% ± 0.11% in the LC, 2.35% ± 0.02% in the IPS, and 2.83% ± 0.03% in the OPS. For the first principal strain, the high strain regions extended out to the IPS. Local high strains were also observed in the LC.

Increasing the load from 20 to 100 kPa increased the strain level by less than 100%, indicating scleral and LC nonlinearity (i.e., stiffening with IOP; Fig. 4). The size of the low strain ring was related to the load magnitude: Larger loads yielded narrower rings. Both the second principal strain (minimum in-plane strain component) and effective strain patterns shared similarities, with a low strain ring in the IPS observed immediately adjacent to the LC insertion site. In the IPS, first principal strain directions were mostly circumferential, while second principal strain directions were mostly meridional.

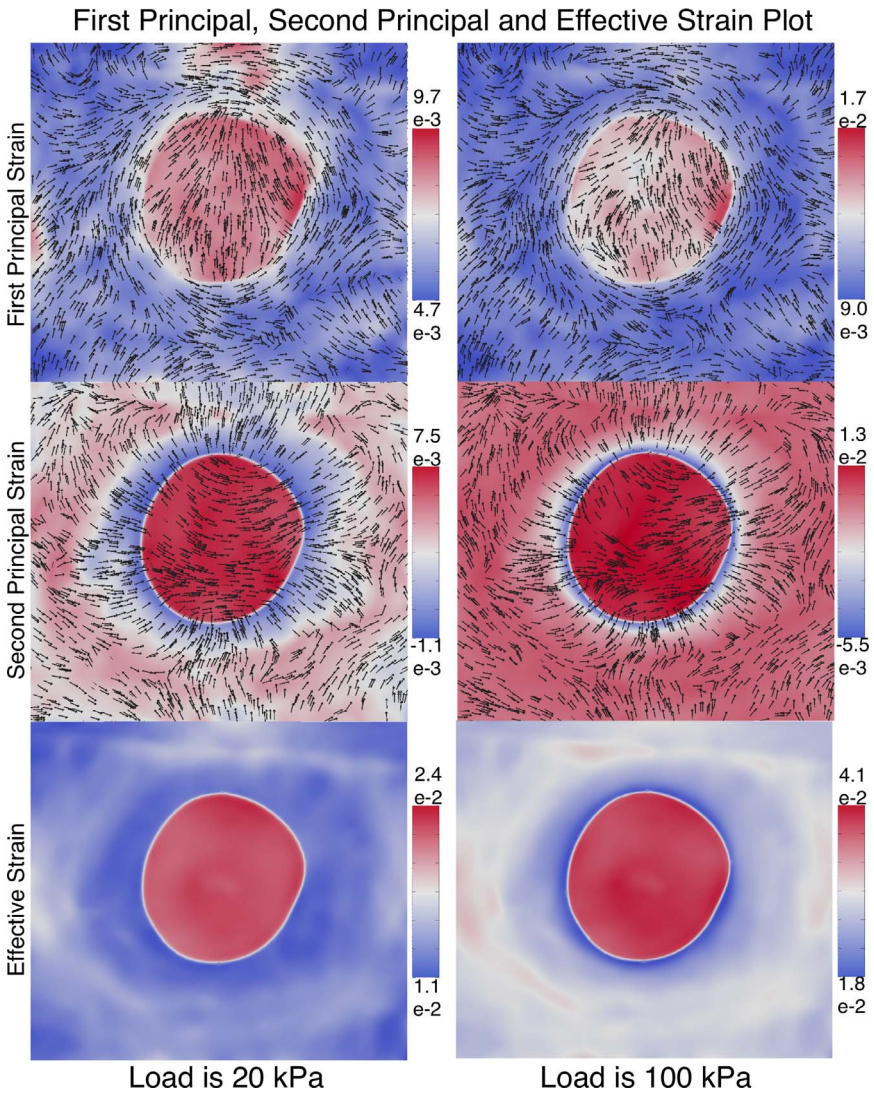

Figure 4. First principal, second principal, and effective strain plots at 20 and 100 kPa loading conditions for a single ONH sample (G1). The *black segments* indicate the principal directions of the strain (first and second principal). The second principal strain pattern resembles the effective strain pattern. In the IPS, the first principal strains are mostly circumferential, representing the scleral canal expansion, while the second principal strains are mostly meridional, representing the radial stretch. In this sense, the low strain ring indicated that the tissue experienced smaller stretch in the radial direction.

Sensitivity Studies

Variations in Fiber Concentration Factor. Fiber concentration factors for the LC or sclera were multiplied by a scaling factor (0, 0.5, or 2). Variations within the sclera had a more prominent impact on IPS, OPS, and LC strain distributions than variations within the LC (Fig. 5a). Violin plots demonstrate strain distributions for a characteristic ONH (G1) sample (Fig. 5b).

In the lamina cribrosa (LC), as the fiber concentration factor was scaled from ×0 to ×2, effective strain (median) decreased slightly in the LC, which was accompanied with an increase in peak strain. A similar trend was observed for the first principal strain. Changing the fiber concentration factors in the LC had no significant influence on strain distributions in the IPS and OPS.

In the sclera, as the fiber concentration factor was scaled from ×0 to ×2, median and peak LC strains decreased significantly (both effective and the first principal strains; mostly $P < 0.001$; Supplementary Fig. S1). The first principal strain in the IPS also decreased significantly ($P < 0.001$; Supplementary Fig. S1). However, the IPS experienced higher peak effective strains even though the median strain decreased. The effective and first principal strain levels increased with increasing scale factor in the OPS.

Variations in Preferred Fiber Orientation. Preferred fiber orientations within the LC and sclera were changed to circumferential or meridional directions. Variations in scleral preferred fiber orientation had more influence on all strain distributions than variations within the LC (Fig. 6a). Violin plots showed the strain distributions for a characteristic ONH (G1) sample (Fig. 6b).

In the lamina cribrosa, changing the preferred fiber orientation from its original configuration (as measured experimentally with SALS) to circumferential or meridional configurations had little influence on strain distributions in the IPS and OPS. Within the LC, the differences were not significant (Supplementary Fig. S2).

In the sclera, changing the preferred fiber orientation from original configuration to meridional configurations had a major

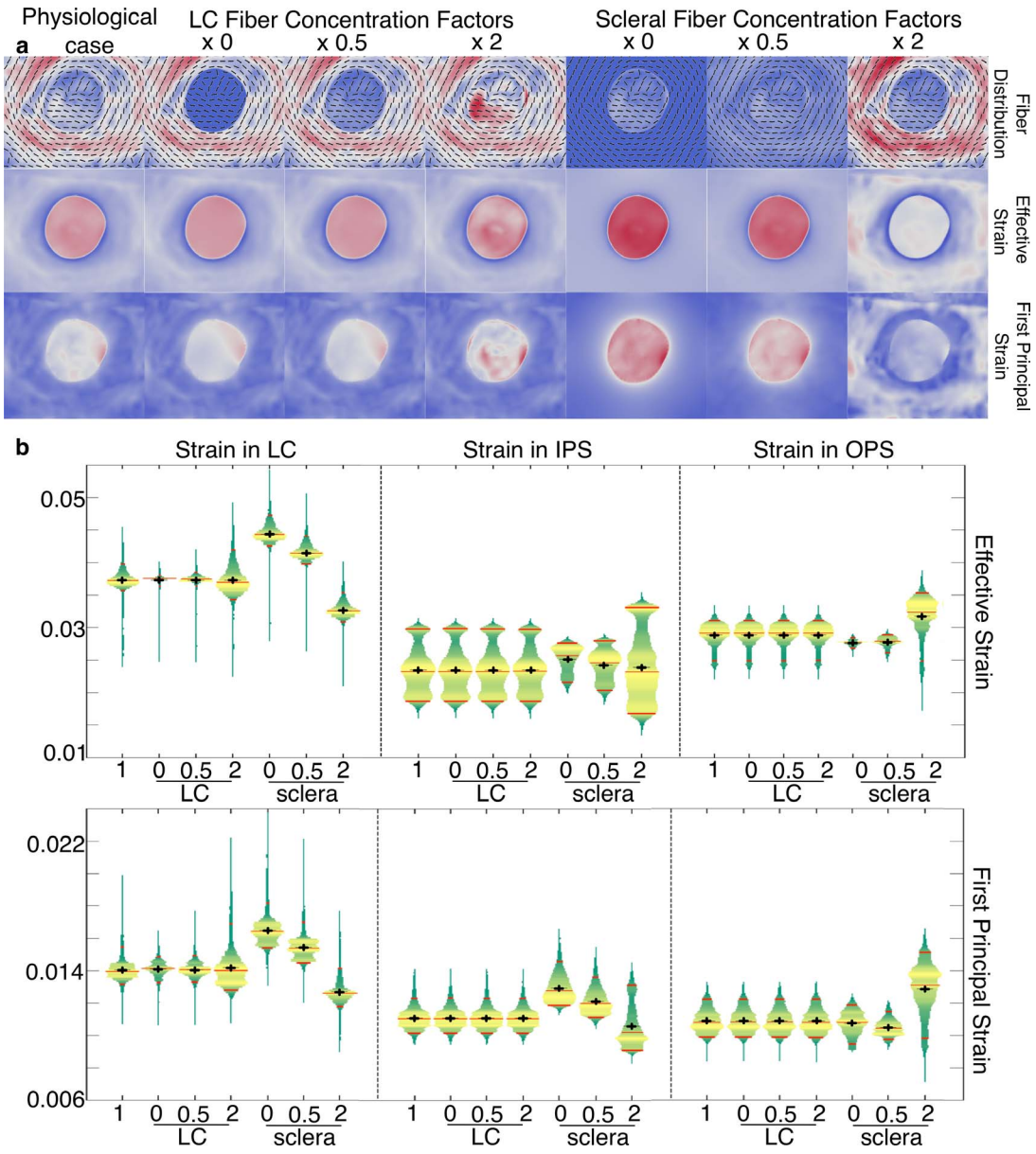

Figure 5. (**a**) Effective strain plots (*second row*) and first principal strain plots (*third row*) due to variations in the LC and scleral anisotropy (*first row*). The physiological case is shown in the *first column* on the left. Starting from the *second column*, the LC fiber concentration factors are multiplied by scaling factors of 0, 0.5, and 2. Starting from the *fifth column*, the scleral fiber concentration factors are similarly multiplied by scaling factors of 0, 0.5, and 2. (**b**) Violin plots of effective strain and first principal strain within the LC, IPS, and OPS, with changes in fiber concentration k for a given ONH sample (G1). Each *plot* represents the strain distribution on the *vertical axis*. The 95th percentile, median, and fifth percentile values are marked with *red line segments*, and the mean value is marked with a *black cross*. Within each region, the strain distributions were obtained from FE simulations in which the fiber concentration factors k within the LC and sclera were multiplied by a factor of 0, 0.5, 1 (unchanged k values), and 2.

influence on LC strain. Specifically, meridional configurations increased LC strain levels by 30.3% (median effective strain, $P < 0.001$; Supplementary Fig. S2) and 33.4% (median first principal strain, $P < 0.001$; Supplementary Fig. S2). Meridional configurations increased the first principal strain level in the sclera; they also increased the effective strain level in the IPS but reduced the peak effective strain in the OPS. On the other hand, changing the preferred fiber orientation to "perfect" circumferential configurations led to less significant changes (Supplementary Fig. S2). Perfect circumferential configurations reduced LC strain levels by 1.25% (median effective strain) and by 1.84% (median first principal strain). Circumferential configurations also led to little changes in IPS and OPS strain levels.

Variations in Stiffness Parameters. Constitutive parameters, namely, c_1, c_3, and c_4, were also varied to investigate the role of fiber and ground substance matrix stiffness (Supplementary Fig. S3). Increasing the stiffness of the ground substance matrix (c_1) and the collagen fiber stiffness (through c_3 and c_4) within the LC yielded lower LC strains (effective and first principal). Increasing the stiffness of the ground substance matrix (c_1) in the sclera yielded higher LC strain levels. Increasing the stiffness of collagen fibers in the sclera uniformly reduced strain levels in all regions.

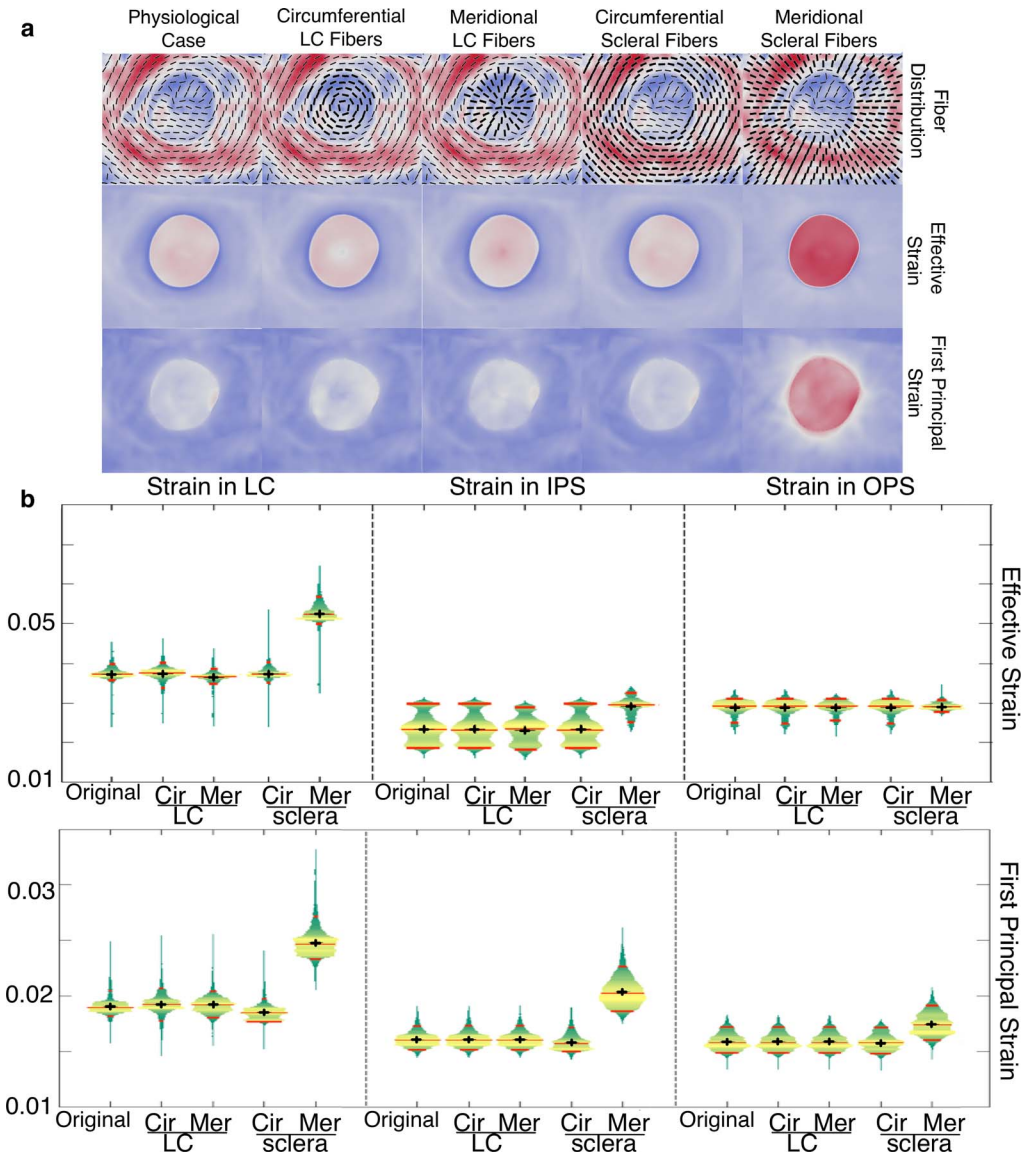

Figure 6. (**a**) Effective strain plots (*second row*) and first principal strain plots (*third row*) with variations in the LC and scleral anisotropy (*first row*). The physiological case is shown in the *first column*, while successive columns show the cases where LC preferred fiber orientations are changed to either circumferential or meridional and scleral preferred fiber orientations are changed to circumferential or meridional. (**b**) Violin plots of effective strain and first principal strain within the LC, IPS, and OPS, with changes in fiber organization (original, circumferential, and meridional) for one ONH sample (G1). Each *plot* represents the strain distribution on the *vertical axis*. The 95th percentile, median, and fifth percentile values were marked with *red line segments*, and the mean value was marked with a *black cross*. Within each region, the strain distributions were obtained from FE simulations using the original microstructure and by changing the preferred fiber orientations within the LC and sclera to obtain circumferential (Cir) and meridional (Mer) organizations.

It was noticed that, as stiffness parameters varied, the low effective strain ring was preserved, and sensitivity analysis results of fiber distributions held true.

Normal Versus Glaucoma ONHs

For ONHs with fiber anisotropy measured by SALS, the normal group had 95th percentile and median effective strain values of 4.09% ± 0.11% and 3.87% ± 0.13% in the LC, while those of the glaucoma group were 4.04% ± 0.10% and 3.90% ± 0.13%; for the first principal strain, the 95th percentile and median values in the LC of the normal group were 1.55% ± 0.03% and 1.43% ± 0.03%, while those of the glaucoma group were 1.58% ± 0.09% and 1.44% ± 0.05%.

Discussion

In this report, we constructed 2D microstructure-based FE models of the human ONH. The fiber microstructural information was experimentally determined from six human postmortem ONHs. We performed sensitivity analyses and evaluated the effect of scleral and LC anisotropy, material nonlinearity, and heterogeneity in collagen fiber organization on simulated IOP-induced strain. Our principal findings are as follows: First, the highest anisotropy was found in the peripapillary sclera not immediately adjacent to, but at a distance (400–500 μm) away from, the scleral canal boundary. Such scleral fiber arrangement reduced the strain in the LC and at the scleral canal boundary. Second, low LC anisotropy and moderate scleral anisotropy (as observed physiologically) act to

limit both LC and scleral strains simultaneously. Third, collagen fiber nonlinear stiffening prominently increased the overall stiffness of the ONH. Fourth, the collagen fiber organization in the peripapillary sclera was the key factor determining the deformation of the LC. Fifth, for our small sample size ($n = 3$), we detected similar LC strain levels in both normal and glaucoma eyes.

Circumferential Scleral Fiber Alignment Reduces Strain at the LC Insertion Sites

In this study, we observed that collagen fibers in the peripapillary sclera formed concentric rings that surrounded the LC and that the highest anisotropy in the peripapillary sclera was observed not immediately adjacent to, but at a distance (400–500 μm) away from the scleral canal (in the OPS region). Circumferential alignment has previously been reported in human,[48–50] porcine,[51] rat,[22] and mouse[52] sclera, but no studies have yet reported variations in fiber concentration factors between the IPS and the OPS.

The direct consequence of a heterogeneous collagen fiber organization in the peripapillary sclera is the presence of rings of low effective and second principal strains at the scleral canal, suggesting that heterogeneous scleral anisotropy provides mechanical protection to the ONH tissues. In the inner peripapillary sclera, first principal strain directions were mostly circumferential, while second principal strain directions were mostly meridional (Fig. 4). The circumferential strain relates to the degree of scleral canal expansion, and the meridional strain relates to the stretch in the radial direction. From this perspective, the low strain ring observed in the second principal strain and in the effective strain might prevent LC disinsertion, focal laminar defects,[53] and optic disc hemorrhages[54] as often observed in glaucoma.

Circumferential fiber arrangement in the peripapillary sclera has been suggested to be the optimum configuration by computational models to match experimental scleral deformation data[23] and to shield the human LC from high stress.[28] In our study, when the scleral fiber concentration factor was increased, the low strain ring at the LC insertion site became more prominent (Fig. 5) and strain levels in the LC and IPS decreased. Furthermore, changing the scleral preferred fiber orientation from circumferential to meridional eliminated the low strain ring (Fig. 6). Based on these facts, we suggest that the low strain ring results from "complex" scleral fiber anisotropy that might act as a self-protective mechanism for the ONH.

A transition zone between the LC and the peripapillary sclera—characterized by low scleral anisotropy and low effective and second principal strain—has not yet been reported in the literature. Most previous computational studies and sensitivity analyses[12–14,55,56] were performed based on the assumption that the eye tissues were linear, isotropic, and homogeneous.[57] A recent study by Coudrillier et al.[24] included experimental data describing fiber anisotropy in the posterior sclera, but this study was limited by the spatial resolution of its fiber measurements. Grytz et al.[30,58] also suggested that the ring of collagen fibers around the LC was crucial to protect the ONH from canal expansion using inflation tests and inverse FE, but the displacement tracking resolution used in their inflation test was not sufficient to capture the strain level immediately adjacent to the LC. Furthermore, the highest anisotropic region of the sclera was predicted immediately adjacent to the scleral canal boundary. Our data suggest that the highest anisotropic region of the sclera is at some distance (400–500 μm) away from the scleral canal boundary and that such a fiber arrangement can reduce effective strains in the LC and at the scleral canal boundary.

Low LC Anisotropy and Moderate Scleral Anisotropy Are Effective Configurations to Reduce LC and Scleral Strains

Our sensitivity analyses suggested that anisotropy is not favored over isotropy in the LC, as high anisotropy increases peak strains significantly (suspected to lead to axonal death[45,59,60]) without reducing the median value. The observed anisotropy level in the LC is relatively low (Fig. 3), which is consistent with this being a biomechanically desirable configuration to maintain low LC peak strains.

Anisotropy in the peripapillary sclera had a notable influence on the strain distributions both in the LC and in the sclera. This conclusion is consistent with Coudrillier's 3D models where the peripapillary sclera was modeled as uniformly anisotropic.[24] Our results clearly showed that higher anisotropy within the peripapillary sclera (with a circumferential arrangement) could significantly reduce strain levels in the LC. However, high anisotropy is not always preferred. Doubling the fiber concentration factors from their physiological values in the sclera yielded a notable increase in median and peak strain levels in the IPS and the OPS. Thus, it seems that neither isotropy nor high anisotropy is optimal for the sclera, and the physiological configuration observed experimentally (moderate anisotropy) appears effective at limiting LC and scleral strains.

Scleral Nonlinear Stiffness Drastically Impacts LC Deformations

Increasing the stiffness of the ground substance matrix or that of the fibers in the LC reduced the LC strain level. While for the sclera, the fiber stiffness was more important. This is consistent with previous studies in the sense that collagen fibers are the main load-bearing structure.[57,61–63] Interestingly, increasing the stiffness of the ground substance matrix in the sclera (from 50 to 200 kPa) slightly increased the LC strain level, as it was equivalent to making the sclera more isotropic.

Collagen Fiber Organization in the Peripapillary Sclera Is a Key Determinant of LC Strain

For all factors discussed above, changes in the sclera always had more prominent influence on the LC than changes in the LC itself. Previous linear elastic models[11–14,55] and nonlinear models[10,24] also ranked peripapillary scleral stiffness as the largest determinant of LC strain. Even though the LC is assumed to be the main site for axonal damage in glaucoma, it is equivalently important to examine the properties of the peripapillary sclera.

LC Strain Levels Were Similar in Both Normal and Glaucoma Eyes

No obvious dissimilarity was detected in LC strain distribution between normal and glaucoma ONHs. There are several possible explanations. First, our sample size was small and not representative as large intersubject variations have been reported for human ocular anatomy[14,64]; second, the FE models assumed a single fiber stiffness value for all ONHs, rather than patient-specific ONH stiffness and heterogeneous variations in fiber stiffness; and third, even though collagen fiber concentration factors and preferred fiber orientations play a critical role in shielding the LC from high strains, they may only vary significantly at certain stages of glaucoma pathogenesis.[34,65,66] Changes in fiber stiffness and density (as observed in aging monkey[23] and human eyes,[67] and monkey eyes subjected to chronic IOP elevation[45]) with the develop-

ment and progression of glaucoma could also be more prominent (as we can observe from the variation of constitutive parameters, fiber stiffness altered the IOP-induced strain drastically). Future work should utilize a larger sample size and include experiments targeted at characterizing the patient-specific fiber stiffness/density together with fiber organization.

Limitations

In this study, several limitations warrant further discussion. First, we performed 2D rather than 3D FE modeling. The generation of 2D models was motivated by the experimental microstructure data as obtained from thick 2D cryosections of human ONHs. As such, our 2D models cannot evaluate the influence of a complex ONH geometry. For instance, idealized 3D computational models have shown that scleral anisotropy could influence the degree of IOP-induced LC bowing[10] and that LC anisotropy could reinforce the LC against high transverse shear stresses and posterior deformations.[28] However, as a large portion of the ONH loads are expected to be in plane, we believe the results from 2D models are meaningful and can provide considerable insight as a first approximation. In fact, the usefulness of 2D modeling for ONH biomechanics has previously been demonstrated. Sander et al.[68] identified the elastic modulus of the sclera and its thickness as the major strain determinants in the LC using 2D cellular solid models. Such results have been consistent with prior 3D FE modeling. Note also that our FE models are the first to incorporate experimental measurements of complex fiber organization in both the LC and the peripapillary sclera of human eyes. Using a simplified 2D approach allows us to understand the direct influence of such heterogeneous collagen fiber organizations while ignoring more complex geometrical effects.

Second, the sectioning plane or the LC within the ONH sample may have been slightly tilted during sectioning. Additionally, the LC may have been cupped. To limit errors, only the central LC portion was incorporated into our analyses. We have also assumed that the LC was inserted into sclera, but LC migration has been suggested in glaucoma eyes.[59,69] In addition, we have assumed that the midposterior sclera had negligible influence over the ONH as it was not included in our models.

Third, our FE models did not include depth-dependent variations in fiber distributions, and as such, our strain predictions may have been affected. A recent study by Pijanka et al.,[25] using multimodal nonlinear microscopy, has shown that fiber concentration factors varied with depth but preferred fiber orientations remained the same. Another study by Danford et al.[66] confirmed depth dependence of the fiber concentration factor in both normal and glaucoma human sclera. More complex FE models will be required to understand the implication of depth-dependent fiber concentration factors on LC and scleral strains.

Fourth, our SALS apparatus operated with a laser beam spot of 300 μm in diameter and, therefore, all the collagen fibers within that area contributed to the fiber distribution at any given scanning point. Since a 300-μm region is large enough to contain a number of fibrillar collagen bundles, we were unable to report anisotropy information at the LC beam level. The main implication is that LC beam strains could not be resolved. However, since we performed overlapping of laser beam regions—which resulted in relatively smooth 2D fiber fields—we believe that our models can still provide insightful information at the continuum level, consistent with our finite element modeling approach.

Fifth, the constitutive parameters we used in the study are results from inverse FE models based on monkey eyes and thus are not exact for human eyes. The corresponding parameters for human sclera and LC have not been reported in the literature, and it is even difficult to incorporate the intersubject difference and intrasubject spatial variation. However, the main target of this study was to investigate the role of fiber concentration and orientation and thus, we kept the constitutive parameters (c_1, c_3, and c_4) constant across different subjects. Note that we have also varied the constitutive stiffness parameters, which should have captured a broader range of IOP-induced mechanical responses.

Sixth, our constitutive model did not describe the pores of the LC as disconnected voids, which may lead to underestimation of the local fiber strain. Nonetheless, LC porosity was still captured at a macroscale by the low LC constitutive parameter values we adopted.

Finally, it is possible that the act of fixation (in 4% paraformaldehyde) might subtly alter scleral and laminar microstructure. We would simply note that fixing whole ONHs, as we have done, is thought to provide tissue samples that suitably reflect the in situ microstructural arrangement of the sclera and LC; further, changes due to fixation have not been reported in any previous SALS study that we are aware of.

Conclusions

The proposed study combined anisotropic, heterogeneous, nonlinear FE models with microstructural data from human eyes and examined the role of collagen fiber concentration and direction in protecting the ONH from excessive IOP-induced stretch. This study showed that circumferentially aligned collagen fibers in the peripapillary sclera yielded low IOP-induced strain rings immediately adjacent to the LC. Fiber concentration and preferred fiber orientation in the peripapillary sclera may be considered as important factors to maintain a suitable biomechanical environment within the LC.

Acknowledgments

The authors thank the Corneal Transplant Service Bristol Eye Bank (Bristol, UK) and Mike Fautsch and the Mayo Clinic (Rochester, NY, USA) for donor research material. Additionally, we thank Nick White (Cardiff University Bioimaging Laboratories) for his expertise and training in SHG imaging.

Supported by the Singapore Ministry of Education Academic Research Funds Tier 1 (R-397-000-181-112; MJAG); NUS Graduate School for Integrative Sciences and Engineering (LZ), Biotechnology and Biological Sciences Research Council (JA); and Cardiff University School of Optometry and Vision Sciences Research Committee (JA).

Disclosure: **L. Zhang**, None; **J. Albon**, None; **H. Jones**, None; **C.L.M. Gouget**, None; **C.R. Ethier**, None; **J.C.H. Goh**, None; **M.J.A. Girard**, None

References

1. Resnikoff S, Pascolini D, Etya'ale D, et al. Global data on visual impairment in the year 2002. *Bull World Health Organ*. 2004; 82:844–851.
2. Balaratnasingam C, Morgan WH, Bass L, Matich G, Cringle SJ, Yu D-Y. Axonal transport and cytoskeletal changes in the laminar regions after elevated intraocular pressure. *Invest Ophthalmol Vis Sci*. 2007;48:3632–3644.
3. Sommer A, Tielsch JM, Katz J, et al. Relationship between intraocular pressure and primary open angle glaucoma among white and black Americans: the Baltimore Eye Survey. *Arch Ophthalmol*. 1991;109:1090–1095.

4. Leske MC, Wu S-Y, Hennis A, Honkanen R, Nemesure B. Risk factors for incident open-angle glaucoma: the Barbados Eye Studies. *Ophthalmology*. 2008;115:85–93.
5. Heijl A, Leske MC, Bengtsson B, Hyman L, Bengtsson B, Hussein M. Reduction of intraocular pressure and glaucoma progression: results from the Early Manifest Glaucoma Trial. *Arch Ophthalmol*. 2002;120:1268–1279.
6. Quigley HA. Glaucoma: macrocosm to microcosm the Friedenwald lecture. *Invest Ophthalmol Vis Sci*. 2005;46: 2663–2670.
7. Burgoyne CF, Crawford DJ, Bellezza AJ, Francis Suh J-KF, Hart RT. The optic nerve head as a biomechanical structure: a new paradigm for understanding the role of IOP-related stress and strain in the pathophysiology of glaucomatous optic nerve head damage. *Prog Retin Eye Res*. 2005;24:39–73.
8. Geijssen HC. *Studies on Normal Pressure Glaucoma*. Amsterdam: Kugler Publications; 1991.
9. Zeimer R. *Biomechanical Properties* of the *Optic Nerve Head. Optic Nerve in Glaucoma*. Amsterdam: Kugler Publications. 1995;107–121.
10. Girard MJA, Downs JC, Burgoyne CF, Suh J-KF. Peripapillary and posterior scleral mechanics–part I: development of an anisotropic hyperelastic constitutive model. *J Biomech Eng*. 2009;131:051011.
11. Sigal IA, Flanagan JG, Tertinegg I, Ethier CR. Finite element modeling of optic nerve head biomechanics. *Invest Ophthalmol Vis Sci*. 2004;45:4378–4387.
12. Norman RE, Flanagan JG, Sigal IA, Rausch SMK, Tertinegg I, Ethier CR. Finite element modeling of the human sclera: influence on optic nerve head biomechanics and connections with glaucoma. *Exp Eye Res*. 2011;93:4–12.
13. Sigal IA, Flanagan JG, Tertinegg I, Ethier CR. Modeling individual-specific human optic nerve head biomechanics. Part I: IOP-induced deformations and influence of geometry. *Biomech Model Mechanobiol*. 2009;8:85–98.
14. Sigal IA, Flanagan JG, Ethier CR. Factors influencing optic nerve head biomechanics. *Invest Ophthalmol Vis Sci*. 2005; 46:4189–4199.
15. Sigal I, Grimm J, Schuman J, Kagemann L, Ishikawa H, Wollstein G. A method to estimate biomechanics and mechanical properties of optic nerve head tissues from parameters measurable using optical coherence tomography. *IEEE Trans Med Imaging*. 2014;33:1381–1389.
16. Girard MJA, Strouthidis NG, Desjardins A, Mari JM, Ethier CR. In vivo optic nerve head biomechanics: performance testing of a three-dimensional tracking algorithm. *J R Soc Interface*. 2013;10:20130459.
17. Sigal IA, Flanagan JG, Tertinegg I, Ethier CR. Reconstruction of human optic nerve heads for finite element modeling. *Technol Health Care*. 2005;13:313–329.
18. Fung Y. *Biomechanics: Mechanical Properties* of *Living Tissues*. New York: Springer-Verlag; 1993.
19. Woo SL, Kobayashi AS, Schlegel WA, Lawrence C. Nonlinear material properties of intact cornea and sclera. *Exp Eye Res*. 1972;14:29–39.
20. Girard MJ, Downs JC, Burgoyne CF, Suh J-KF. Experimental surface strain mapping of porcine peripapillary sclera due to elevations of intraocular pressure. *J Biomech Eng*. 2008;130: 041017.
21. Spoerl E, Boehm AG, Pillunat LE. The influence of various substances on the biomechanical behavior of lamina cribrosa and peripapillary sclera. *Invest Ophthalmol Vis Sci*. 2005;46: 1286–1290.
22. Girard MJA, Dahlmann-Noor A, Rayapureddi S, et al. Quantitative mapping of scleral fiber orientation in normal rat eyes. *Invest Ophthalmol Vis Sci*. 2011;52:9684–9693.
23. Girard MJA, Suh J-KF, Bottlang M, Burgoyne CF, Downs JC. Scleral biomechanics in the aging monkey eye. *Invest Ophthalmol Vis Sci*. 2009;50:5226–5237.
24. Coudrillier B, Boote C, Quigley HA, Nguyen TD. Scleral anisotropy and its effects on the mechanical response of the optic nerve head. *Biomech Model Mechanobiol*. 2013;12: 941–963.
25. Pijanka JK, Coudrillier B, Ziegler K, et al. Quantitative mapping of collagen fiber orientation in non-glaucoma and glaucoma posterior human sclerae. *Invest Ophthalmol Vis Sci*. 2012;53: 5258–5270.
26. Grytz R, Meschke G. Constitutive modeling of crimped collagen fibrils in soft tissues. *J Mech Behav Biomed Mater*. 2009;2:522–533.
27. Campbell IC, Coudrillier B, Mensah J, Abel RL, Ethier CR. Automated segmentation of the lamina cribrosa using Frangi's filter: a novel approach for rapid identification of tissue volume fraction and beam orientation in a trabeculated structure in the eye. *J R Soc Interface*. 2015;12:20141009.
28. Grytz R, Meschke G, Jonas JB. The collagen fibril architecture in the lamina cribrosa and peripapillary sclera predicted by a computational remodeling approach. *Biomech Model Mechanobiol*. 2011;10:371–382.
29. Grytz R, Meschke G. A computational remodeling approach to predict the physiological architecture of the collagen fibril network in corneo-scleral shells. *Biomech Model Mechanobiol*. 2010;9:225–235.
30. Grytz R, Fazio MA, Girard MJA, et al. Material properties of the posterior human sclera. *J Mech Behav Biomed Mater*. 2013;1–16.
31. Grytz R, Downs JC. A forward incremental prestressing method with application to inverse parameter estimations and eye-specific simulations of posterior scleral shells. *Comput Methods Biomech Biomed Engin*. 2011;1–13.
32. Girard MJA, Downs JC, Bottlang M, Burgoyne CF, Suh J-KF. Peripapillary and posterior scleral mechanics–part II: experimental and inverse finite element characterization. *J Biomech Eng*. 2009;131:051012.
33. Watson PG, Young RD. Scleral structure, organisation and disease. A review. *Exp Eye Res*. 2004;78:609–623.
34. Roberts MD, Grau V, Grimm J, et al. Remodeling of the connective tissue microarchitecture of the lamina cribrosa in early experimental glaucoma. *Invest Ophthalmol Vis Sci*. 2009;50:681–690.
35. Kronick PL, Sacks MS. Quantification of vertical-fiber defect in cattle hide by small-angle light scattering. *Connect Tissue Res*. 1991;27:1–13.
36. Chien JC, Chang E. Small-angle light scattering of reconstituted collagen. *Macromolecules*. 1972;5:610–617.
37. Sacks MS, Smith DB, Hiester ED. A small angle light scattering device for planar connective tissue microstructural analysis. *Ann Biomed Eng*. 1997;25:678–689.
38. Gouget CLM, Girard MJ, Ethier CR. A constrained von Mises distribution to describe fiber organization in thin soft tissues. *Biomech Model Mechanobiol*. 2012;11:475–482.
39. Price K, Storn RM, Lampinen JA. *Differential Evolution: A Practical Approach to Global Optimization*. Berlin: Springer; 2006.
40. Ferdman AG, Yannas IV. Scattering of light from histologic sections: a new method for the analysis of connective tissue. *J Invest Dermatol*. 1993;100:710–716.
41. Abahussin M, Hayes S, Cartwright NEK, et al. 3D collagen orientation study of the human cornea using x-ray diffraction and femtosecond laser technology. *Invest Ophthalmol Vis Sci*. 2009;50:5159–5164.

Investigative Ophthalmology & Visual Science

42. Fisher NI. *Statistical Analysis of Circular Data*. Cambridge: Cambridge University Press; 1995.
43. Gasser TC, Ogden RW, Holzapfel GA. Hyperelastic modelling of arterial layers with distributed collagen fibre orientations. *J R Soc Interface*. 2006;3:15–35.
44. Bellezza AJ, Hart RT, Burgoyne CF. The optic nerve head as a biomechanical structure: initial finite element modeling. *Invest Ophthalmol Vis Sci*. 2000;41:2991–3000.
45. Girard MJA, Suh J-KF, Bottlang M, Burgoyne CF, Downs JC. Biomechanical changes in the sclera of monkey eyes exposed to chronic IOP elevations. *Invest Ophthalmol Vis Sci*. 2011;52:5656–5669.
46. Weiss JA, Maker BN, Govindjee S. Finite element implementation of incompressible, transversely isotropic hyperelasticity. *Comput Methods Appl Mech Eng*. 1996;135:107–128.
47. Maas SA, Ellis BJ, Rawlins DS, Weiss JA. A comparison of FEBio, ABAQUS, and NIKE3D. Results for a suite of verification problems. Salt Lake City, UT: University of Utah Scientific Computing and Imaging Institute. Published December 1, 2009. Available at: https://www.sci.utah.edu/publications/SCITechReports/UUSCI-2009-009.pdf. Accessed May 22, 2014.
48. Kokott W. Das spaltlinienbild der sklera. (Ein beitrag zum funktionellen bau der sklera). *Klin Monbl Augenheilkd*. 1934;92:177–185.
49. Winkler M, Jester B, Nien-Shy C, et al. High resolution three-dimensional reconstruction of the collagenous matrix of the human optic nerve head. *Brain Res Bull*. 2010;81:339–348.
50. Hernandez MR, Luo XX, Igoe F, Neufeld A. Extracellular matrix of the human lamina cribrosa. *Am J Ophthalmol*. 1987;104:567–576.
51. Kokott W. Über mechanisch-funktionelle Strukturen des Auges. *Graefes Arch Clin Exp Ophthalmol*. 1938;138:424–485.
52. May CA, Lütjen-Drecoll E. Morphology of the murine optic nerve. *Invest Ophthalmol Vis Sci*. 2002;43:2206–2212.
53. Kiumehr S, Park SC, Syril D, et al. In vivo evaluation of focal lamina cribrosa defects in glaucoma. *Arch Ophthalmol*. 2012;130:552–559.
54. Lee EJ, Kim T-W, Kim M, Girard MJ, Mari JM, Weinreb RN. Recent structural alteration of the peripheral lamina cribrosa near the location of disc hemorrhage in glaucoma. *Invest Ophthalmol Vis Sci*. 2014;55:2805–2815.
55. Sigal IA, Ethier CR. Biomechanics of the optic nerve head. *Exp Eye Res*. 2009;88:799–807.
56. Sigal IA, Flanagan JG, Tertinegg I, Ethier CR. Predicted extension, compression and shearing of optic nerve head tissues. *Exp Eye Res*. 2007;85:312–322.
57. Grytz R, Girkin CA, Libertiaux V, Downs JC. Perspectives on biomechanical growth and remodeling mechanisms in glaucoma. *Mech Res Commun*. 2012;42:92–106.
58. Fazio MA, Grytz R, Bruno L, et al. Regional variations in mechanical strain in the posterior human sclera. *Invest Ophthalmol Vis Sci*. 2012;53:5326–5333.
59. Crawford DJ, Roberts MD, Sigal IA. Glaucomatous cupping of the lamina cribrosa: a review of the evidence for active progressive remodeling as a mechanism. *Exp Eye Res*. 2011;93:133–140.
60. Agoumi Y, Sharpe GP, Hutchison DM, Nicolela MT, Artes PH, Chauhan BC. Laminar and prelaminar tissue displacement during intraocular pressure elevation in glaucoma patients and healthy controls. *Ophthalmology*. 2011;118:52–59.
61. Brown DJ, Morishige N, Neekhra A, Minckler DS, Jester JV. Application of second harmonic imaging microscopy to assess structural changes in optic nerve head structure ex vivo. *J Biomed Opt*. 2013;12:024029.
62. Albon J, Purslow PP, Karwatowski WS, Easty DL. Age related compliance of the lamina cribrosa in human eyes. *Br J Ophthalmol*. 2000;84:318–323.
63. Albon J, Karwatowski WS, Easty DL, Sims TJ, Duance VC. Age related changes in the non-collagenous components of the extracellular matrix of the human lamina cribrosa. *Br J Ophthalmol*. 2000;84:311–317.
64. Eilaghi A, Flanagan JG, Simmons CA, Ethier CR. Effects of scleral stiffness properties on optic nerve head biomechanics. *Ann Biomed Eng*. 2010;38:1586–1592.
65. Pijanka JK, Coudrillier B, Ziegler K, et al. Quantitative mapping of collagen fiber orientation in non-glaucoma and glaucoma posterior human sclerae. *Invest Ophthalmol Vis Sci*. 2012;53:5258–5270.
66. Danford FL, Yan D, Dreier RA, Cahir TM, Girkin CA, Geest JPV. Differences in the region-and depth-dependent microstructural organization in normal versus glaucomatous human posterior sclerae. *Invest Ophthalmol Vis Sci*. 2013;54:7922–7932.
67. Schultz DS, Lotz JC, Lee SM, Trinidad ML, Stewart JM. Structural factors that mediate scleral stiffness. *Invest Ophthalmol Vis Sci*. 2008;49:4232–4236.
68. Sander E, Downs J, Hart R, Burgoyne C, Nauman E. A cellular solid model of the lamina cribrosa: mechanical dependence on morphology. *J Biomech Eng*. 2006;128:879–889.
69. Sigal IA, Bilonick RA, Kagemann L, et al. The optic nerve head as a robust biomechanical system. *Invest Ophthalmol Vis Sci*. 2012;53:2658–2667.

Investigative Ophthalmology & Visual Science